

Modeling intermediate band solar cells: a roadmap to high efficiency

Jacob J. Krich,^a Anna H. Trojnar,^a Liang Feng,^b Karin Hinzer,^a and Alexandre W. Walker^a

^a University of Ottawa, Ottawa, ON, Canada;

^b Nanjing University, Nanjing, China

ABSTRACT

Intermediate band (IB) photovoltaics have the potential to be highly efficient and cost effective solar cells. When the IB concept was proposed in 1997, there were no known intermediate band materials. In recent years, great progress has been made in developing materials with intermediate bands, though power conversion efficiencies have remained low. To understand the material requirements to increase IB device efficiencies, we must develop good models for their behavior under bias and illumination. To evaluate potential IB materials, we present a figure of merit, consisting of parameters that can be measured without solar cell fabrication. We present a new model for IB devices, including the behavior of their junctions with n- and p-type semiconductors. Using a depletion approximation, we present analytic approximations for the boundary conditions of the minority carrier diffusion equations. We compare the analytic results to Synopsys Sentaurus device models. We use this model to find the optimal thickness of the IB region based on material parameters. For sufficiently poor IB materials, the optimal thickness is zero – i.e., the device is more efficient without the IB material at all. We show the minimum value of the figure of merit required for an IB to improve the efficiency of a device, providing a clear goal for the quality of future IB materials.

Keywords: Photovoltaics, intermediate band, device modeling

1. INTRODUCTION

Standard solar cells made from a single semiconductor pn junction are the overwhelming majority of the rapidly expanding solar industry. Shockley and Queisser showed that such an architecture has a theoretical maximum efficiency of 32% in unconcentrated sunlight or 41% in concentrated sunlight, since semiconductors can absorb only photons of energy greater than their band gap, lose any excess photon energy to thermalization, and must have radiative recombination processes.¹ There have been many efforts to exceed the Shockley-Queisser limit, with experimental success achieved by multijunction solar cells.² There are a number of other high-efficiency concepts (including hot carrier, multiple exciton generation, upconversion, and downconversion³), none of which has achieved experimental efficiency exceeding the Shockley-Queisser limit.

In 1997, Luque and Martí proposed another high-efficiency concept, the intermediate band solar cell (IBSC).⁴ The IBSC is a p -IB- n structure, with the p - and n -type regions formed from a large-bandgap semiconductor (band gap ideally 1.9 eV) and the intermediate band (IB) region consisting of a modified semiconductor with a large band gap and an extra set of allowed electronic levels entirely contained inside the band gap, illustrated in Fig. 1. The extra levels in the IB region allow absorption of sub-band gap photons, which promote an electron from the valence band (VB) to the IB and from the IB to the conduction band (CB). In ideal conditions, the voltage is still determined by the band gap of the surrounding p - and n -type materials, allowing an increase in current compared to the Shockley-Queisser limit. Under full concentration, such a device has an efficiency limit of 63%, equivalent to an ideal triple-junction cell.

In 1997, there were no known materials that had such a band structure. Semiconductor quantum dots such as InAs in GaAs provide a band structure similar to that required for IBSC and have been widely studied.⁵ More recently, a number of engineered semiconductor systems have been reported to display the IB band structure. The most widely studied is the class of highly-mismatched alloys, including dilute nitrides^{6,7} and ZnTe:O.^{8,9}

Send correspondence to jkrich@uottawa.ca. A.W.W. current address: Fraunhofer ISE, Freiburg, Germany.

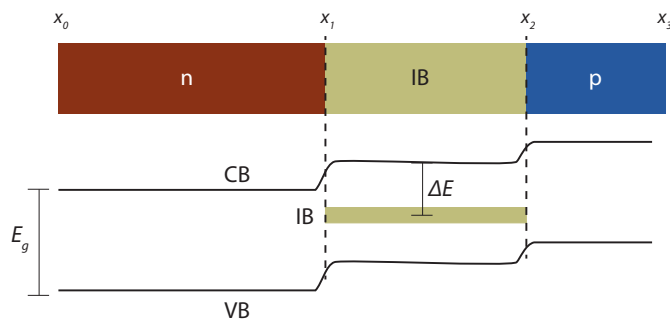


Figure 1. Sketch of an intermediate band solar cell showing the n -, IB, and p -type regions and the associated valence band (VB) and conduction band (CB) edges, with flat-band conditions applying in all three bulk regions of the sample. The IB region material has an extra set of levels an energy ΔE below the CB. The interface positions are labeled as x_i for i from 0 to 3.

Silicon heavily doped with a range of deep-level-forming impurities has also been studied,^{10–19} and there are a number of theoretical proposals of crystalline materials with IB band structures.^{20–25} The efficiencies of IBSC devices remain low, generally less than 1%, which may be due to fast nonradiative recombination through the IB.^{6,8} Progress in improving the efficiency of IBSC devices requires that we have good models of carrier transport, to allow predictions and optimizations of device performance. In this paper, we present progress toward a one-dimensional model for the uncoupled equations of motion of electrons and holes in an IB device. We verify the boundary conditions using the commercial device modeling software TCAD Sentaurus, which solves the coupled electron and hole transport equations but cannot model the IB absorption processes. Given fixed material properties for an IB material (absorption coefficients, carrier lifetimes, mobilities, etc.), we use our model to determine the optimal thickness of the IB layer and to find the maximum efficiency IBSC device that can be built. We conclude that a simple figure of merit gives a good indication of when an IB material is of sufficient quality to produce high-efficiency solar cells.

2. FIGURE OF MERIT

Creating useful solar cells involve sometimes difficult growth and fabrication issues; power conversion efficiencies can be limited by issues such as contacts and interfaces. For a still-novel architecture such as IBSC, it is helpful to have figures of merit to characterize the quality of the absorber material alone. A figure of merit for IB absorber materials ν was proposed in Ref. 26 and has been measured in one candidate material.²⁷ The figure of merit is the ratio, in a device of optimal IB thickness, of the lifetime τ of an electron in the IB region to the transit time t for an electron to cross the IB region. In the case of a solar cell where there is a static electric field throughout the IB region (as in the intrinsic region of a p - i - n device), so the carriers primarily move by drift, ν can be written as

$$\nu_{\text{drift}} = \frac{E_g}{q} \alpha^2 \mu \tau, \quad (1)$$

where E_g is the band gap, q is the electric charge, α is the mean sub-gap absorptivity in the IB region, and μ is the carrier mobility.* As α increases, the IB region can be made thinner, allowing lower-quality materials (measured by $\mu\tau$) to be effective. There are two figures of merit, one each for electrons and for holes; note that both electrons and holes can be considered minority carriers in the IB region. In the case that the IB region is flat-band, i.e., has no electric field, the carriers must diffuse and the figure of merit is smaller, becoming

$$\nu_{\text{diff}} = \frac{k_b T}{q} \alpha^2 \mu \tau,$$

*Reference 26 had the built-in voltage V_{bi} in place of E_g/q . But since $V_{bi} \leq E_g/q$ and E_g is a material property independent of the doping of the surrounding material, it is preferable to use E_g/q .

where k_b is Boltzmann's constant and T is the temperature. Using the Einstein relation, $\nu_{\text{diff}} = (L\alpha)^2$, where L is the diffusion length.

These figures of merit involve only measurable parameters of the IB absorber material and thus can be determined without solar cell fabrication. They clearly do not capture all of the requirements for efficient IBSC as they do not depend on the IB energy level and thus its matching to the solar spectrum. Measurement of ν for candidate IB materials can screen whether they can make efficient devices. The figure of merit has been measured in one experimental system, silicon highly doped with sulfur, finding $\nu_{\text{drift}} < 0.2$ for electrons at 36 K.^{27†}

3. DEVICE MODEL

We now introduce a device model in order to evaluate, as a function of ν , what efficiency we can expect from an IBSC device of particular band gaps. A number of previous device models for IBSC have been produced,²⁸⁻³³ including different levels of detailed balance, carrier transport, and recombination. Those that model carrier transport assume that there is a static electric field in the IB region, as is appropriate for an IB created by quantum dots (due to their low concentration) or an IB that has no carriers at equilibrium. The ideal IB is half-filled at equilibrium and has a large number of states (to maximize absorption in a thin layer – α^2 in the figure of merit), and such a material should produce a flat-band, no-electric-field condition in the intermediate band, as in Fig. 1. Here we introduce a model for the case of such a flat-band device, and we will focus on ν_{diff} , which we will call ν . We will present full details of the model in a later publication.

At the interface between the n - and IB-type materials, the IB behaves like the p -type side of an np junction. Electrons move from the n -type material to fill empty states in the IB, producing a built-in voltage V_{bi}^{NI} . Making a depletion approximation, where the donors and ionized (filled) IB states are the only source of charge density in this region, one can calculate depletion widths in a similar fashion to the np junction;³⁴ for the case of a heavily-doped n -type material and an IB with a large density of states, the junctions will be thin. For analytic purposes, we approximate the junctions as infinitely narrow (i.e., no generation or recombination in the depletion region), but see Fig. 2 for a more realistic estimate. Similar assumptions were made at the IB- p junction. For simplicity, we assume that the n -type region has a single absorption coefficient α_{CV} for all photon energies above E_g . The IB region has two absorption coefficients, α_{IV} , α_{CI} for absorptions from VB to IB and IB to CB, respectively. We consider an IB at a single energy $\Delta E < E_g/2$ below the CB edge, as in Fig. 1. As is usual, we assume that photons with energy between ΔE and $E_g - \Delta E$ entirely promote from IB to CB and those between $E_g - \Delta E$ and E_g entirely promote VB to IB. These absorptions must be current matched for maximum efficiency.

In the n - and IB-type regions, the holes obey the minority carrier diffusion equation with diffusion constants D_{pN} and D_{pI} , respectively. Similarly for electrons in the IB- and p -type regions.

$$D_{pX} \frac{\partial^2 \Delta p}{\partial x^2} - \frac{\Delta p}{\tau_{pX}} = -G_{pX}(x)$$

$$D_{nX} \frac{\partial^2 \Delta n}{\partial x^2} - \frac{\Delta n}{\tau_{nX}} = -G_{nX}(x)$$

for $X \in \{N, I, P\}$. The lifetimes τ_{cX} include radiative and nonradiative processes. We define diffusion lengths $L_{cX} = \sqrt{D_{cX}\tau_{cX}}$ for $c \in \{p, n\}$ and $X \in \{N, I, P\}$. The generation rates are modeled as

$$G_{pN}(x) = I_{CV}\alpha_{CV}e^{-\alpha_{CV}(x-x_0)}$$

$$G_{pI}(x) = I_{IV}\alpha_{IV}e^{-\alpha_{IV}(x-x_1)}$$

$$G_{nI}(x) = I_{CI}\alpha_{CI}e^{-\alpha_{CI}(x-x_1)}$$

$$G_{nP}(x) = 0,$$

where I_{CV} is the incident photon flux with photon energy greater than E_g , I_{IV} is the incident photon flux with photon energy between $E_g - \Delta E$ and E_g , and I_{CI} is the incident photon flux with photon energy between ΔE and $E_g - \Delta E$. To determine the maximal efficiency attainable with fixed ν , we assume that the n - and p -type

[†]Reference 27 reported $\nu < 0.05$ but used a definition of ν that differed by a factor of 4 from Eq. 1.

regions are essentially ideal, with $\frac{L_{pN}}{l_N}, \frac{L_{nP}}{l_P}, \alpha_{CV}l_N \gg 1$, where $l_N = x_1 - x_0$ and $l_P = x_3 - x_2$ (with reference to Fig. 1), and minority-carrier surface recombination velocities of zero at the front and back contacts, so all of the above-gap light is absorbed in the emitter and essentially all of the carriers make it to the junction with the IB materials. In keeping with the simplicity of the model, we take the incident solar spectrum to be from a black body at temperature 6000 K and consider full concentration of 46,500 suns. With an applied bias V_{app} placed across the device, we must determine how much of it drops across the n -IB junction and how much across the IB- p junction. As in any circuit at steady state, the total electrical current must be uniform, so we determine the separate voltage drops by requiring that the currents $J_p(x_1) + J_n(x_1) = J_p(x_2) + J_n(x_2)$.

To solve this system, we need eight boundary conditions at the interfaces x_i . We set minority-carrier surface recombination velocities to zero at x_0 and x_3 , modeling an ideal cell with a front-surface and back-surface field. In keeping with our thin-junction approximation, we set the hole current J_p to be constant across x_1 and the electron current J_n to be constant across x_2 . We use a modified version of the law of the junction³⁵ for $\Delta n(x_1^+)$ and $\Delta p(x_2^-)$ and to relate $\Delta p(x_1^-)$ to $\Delta p(x_1^+)$ and $\Delta n(x_2^-)$ to $\Delta n(x_2^+)$. We take

$$\begin{aligned}\Delta n(x_1^+) &= n_{0I}(e^{qV_{NI}/k_bT} - 1) \\ \Delta p(x_2^-) &= p_{0I}(e^{qV_{IP}/k_bT} - 1) \\ \Delta p(x_1^-) &= p_{0N}(e^{qV_{NI}/k_bT} - 1) + \Delta p(x_1^+) \frac{p_{0N}}{p_{0I}} e^{qV_{NI}/k_bT} \\ \Delta n(x_2^+) &= n_{0P}(e^{qV_{IP}/k_bT} - 1) + \Delta n(x_2^-) \frac{n_{0P}}{n_{0I}} e^{qV_{IP}/k_bT} \\ n(x_2^+) &= n(x_2^-) \frac{n_{0P}}{n_{0I}} e^{qV_{IP}/k_bT}\end{aligned}\tag{2}$$

$$\tag{3}$$

where $n_{0P}, n_{0I}, p_{0I}, p_{0N}$ are the equilibrium concentrations of electrons and holes in the p -type region, IB region and n -type regions and V_{NI}, V_{IP} are the voltage drops across the n -IB and IB- p junctions, respectively. Future work will derive these conditions and discuss modifications to them and their range of validity. For use in Sec. 4, we provide Eq. 3, which is a rewriting of Eq. 2. In the next section we use comparisons with more sophisticated device modeling software to justify these boundary conditions. Together, these conditions suffice to give $J(V)$ and the power conversion efficiency η .

4. JUSTIFICATION OF BOUNDARY CONDITIONS WITH TCAD SENTAURUS

The proposed boundary conditions were compared with the results of numerical calculations performed using the TCAD Sentaurus package (version vG-2012.06) from Synopsys Inc. – a commercially available semiconductor device simulation package capable of solving the Poisson equation coupled to the electron and hole current-continuity equations at all mesh points of a given structure.³⁶ The numerical calculations consist of two steps: first, a transfer-matrix method is used to calculate optical reflection and depth-dependent intensity, allowing to compute the optical generation (absorption) within each layer of the junction. Second, the calculated optical generation is used as an input to the main equation solver, where the coupled Poisson and drift-diffusion equations are solved. These equations take into account the important semiconductor quantities such as mobilities, Fermi statistics for carrier concentrations, electron and hole effective masses, their corresponding effective conduction and valence band density of states, generation, and recombination phenomena. To calculate a J - V curve, the equations are solved repeatedly as the bias on the contacts is swept over a range of voltages. Similar modeling was performed in Refs. 37-38.

For the results presented below, the n -IB- p structure is discretized in a 1D grid representing a symmetry element of the complete junction based on the assumption that no significant effects occur at the edges of the junction. We have modeled a simplified version of GaAs with a goal of testing the boundary conditions of Section 3 rather than modeling a particular material. The band gap of all regions was taken to be 1.42 eV. In the n - and p -type regions, respectively, $N_D = N_A = 10^{17} \text{ cm}^{-3}$. The IB layer was modeled by introduction of additional half-filled allowed energy levels (traps) with $\Delta E = 0.27 \text{ eV}$. These states are constructed from additional donors and acceptor traps of equal concentration 10^{18} cm^{-3} with scattering cross section of 10^{-16} cm^2 , but no Shockley-Read-Hall recombination was included. The simulations were performed at 298 K device temperature.

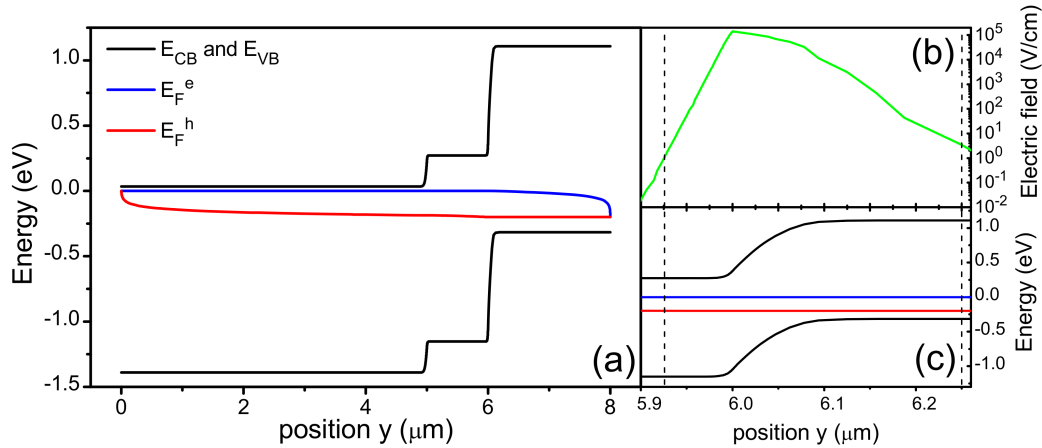


Figure 2. (a) Band diagram of n -IB- p junction with applied voltage $V=0.2$ V. The quasi-Fermi levels for electrons E_{fe} and holes E_{fh} are clearly split. Two depletion regions are clearly established at the junctions, with flat-band conditions between. (b) Electric field near the IB- p junction. Dashed vertical lines denote the limits of the depletion region, which extends mostly into the p -type side, determined as the points where $E = 1$ V/cm. (c) Close up of the band diagram near the IB- p junction.

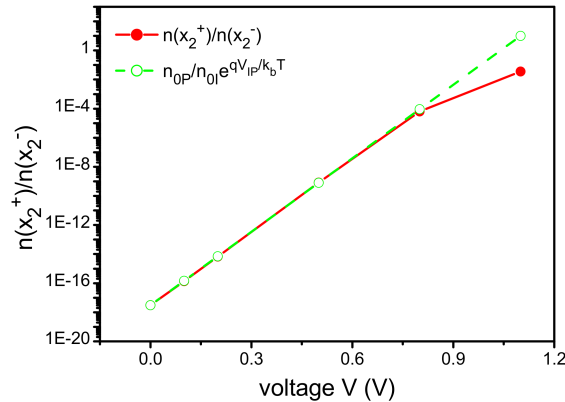


Figure 3. Comparison of Eq. 3 to the results from the Sentaurus simulations in the dark. The analytic result is highly accurate until the voltage approaches the built-in voltage across the device, approximately 1.3V. The applied voltage drops almost entirely across the IB- p junction, because the IB is closer to the CB than the VB.

The hole and electron mobilities have been set as constant in each region (with no doping or concentration dependence). The n - and p -region electron and hole mobilities were set to $\mu_e = 8557 \text{ cm}^2\text{V}^{-1}\text{s}^{-1}$ and $\mu_h = 1620 \text{ cm}^2\text{V}^{-1}\text{s}^{-1}$, respectively; μ_e is the Sentaurus default for GaAs while we have increased μ_h from the default by a factor of 4. In the IB layer the mobilities are $\mu_e = 9533 \text{ cm}^2\text{V}^{-1}\text{s}^{-1}$ and $\mu_h = 500 \text{ cm}^2\text{V}^{-1}\text{s}^{-1}$, chosen from the model of Ref. 39.

The only recombination process considered is radiative recombination, while thermionic emission is included to allow carrier transport across small barriers at heterointerfaces. Since Sentaurus does not permit simulation of the optical absorption due to the traps that create the IB, we present results from Sentaurus only in the dark.

The band structure of the device is shown in Fig. 2a with an applied bias of 0.2 V. The flat-band condition is clearly followed. Figs. 2b,c show the size of the depletion region for this case and that it extends mostly into the (more lightly doped) semiconductor region. Figure 3 shows that Eq. 3 is obeyed with high precision until the voltage approaches the built-in voltage. Similar agreement is found for the other analytic boundary conditions, which gives us confidence that the analytic model is able to describe this type of device accurately.

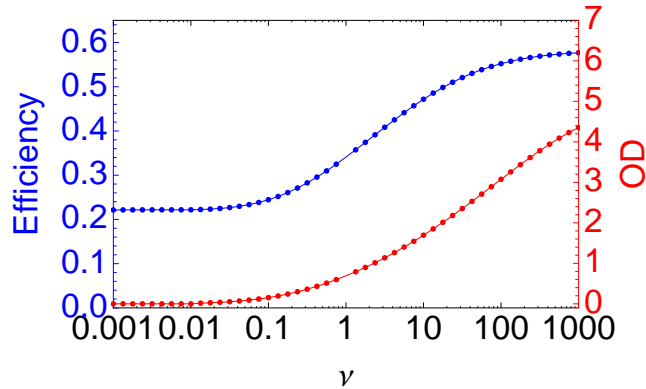


Figure 4. Maximum efficiency and optical depth (OD) of the IB region as a function of figure of merit ν of a system with parameters described in the main text. The OD at highest efficiency is essentially zero at low ν , indicating that the device is better without the IB at all. As ν approaches 1, OD becomes non-negligible.

5. RESULTS

We applied the analytical model of Sec. 3 to study a system with the ideal IB band gaps under full concentration, $E_g = 1.9$ eV and $\Delta E = 0.7$ eV.⁴ The precise values of the material parameters chosen are not essential – the interesting part of this model is the dependence of η on ν . We chose the system to have identical electron and hole transport and recombination properties, except for radiative recombination, with $N_A = N_D = 10^{17}$ cm⁻³ in the p - and n -type sides, $\alpha_{IC} = \alpha_{VI} \equiv \alpha_I$ and $L_{pI} = L_{nI} \equiv L_I$. We calculate the radiative lifetimes τ_r in the usual way³⁴ and include a nonradiative lifetime $\tau_{nr} = 1$ μ s for both electrons and holes, with $\tau^{-1} = \tau_r^{-1} + \tau_{nr}^{-1}$. We fix $\alpha_I = 1$ μ m⁻¹, $L_I = \sqrt{\nu}/\alpha_I$. We characterize the IB by its optical depth $OD = \alpha_I(x_2 - x_1)$, which we vary to find the optimum efficiency for fixed ν . The IB is taken to be half-filled outside the depletion regions.

Figure 4 shows the optimized OD and resulting maximum power conversion efficiency η as a function of figure of merit ν for this model. For small ν , the efficiency is 22% and the optimum cell has an IB OD of essentially zero; that is, the highest efficiency cell has no IB at all. As ν increases, the ideal cell has a larger IB region and increasing efficiency. The turn-on is somewhere between $\nu = 0.1$ and $\nu = 1$, with significant improvements in efficiency possible for $\nu > 1$. Note that for $OD < 0.14$ (which occurs for $\nu \lesssim 0.07$), in these simulations the IB is thinner than the depletion regions found in Sec. 4, so these results should be disregarded, as the flat-band condition cannot apply.

We conclude that IB materials should have $\nu \gtrsim 1$ before it is worthwhile to build PV devices and expect an improvement in efficiency compared to a device without an IB.

6. CONCLUSIONS

We introduce an analytical model for IBSC devices in the diffusive (flat-band) limit and check the validity (in the dark) of its approximate boundary conditions using simulations in the commercial modeling package TCAD Sentaurus. We use a simple figure of merit ν to describe the potential of IB absorber layers and find that until ν approaches 1, there is no efficiency gain produced by the IBSC architecture, for the case of band gaps optimally matched to the fully-concentrated solar spectrum and ideal p and n regions. We believe that measurements of ν for candidate IB materials, as in Ref. 27, are an excellent way to screen the quality of such materials before building devices. Once ν is known (for both electrons and holes) in the absorber material, a model as presented here can predict the optimal thickness for maximum power conversion efficiency.

ACKNOWLEDGMENTS

We acknowledge valuable discussions with Michael Nesrallah, Nicholas Rogers, and Matthew Wilkins, and support from NSERC, the Photovoltaic Innovation Network, and MITACS Globalink.

REFERENCES

1. Shockley, W. and Queisser, H. J., "Detailed balance limit of efficiency of p-n junction solar cells," *J. Appl. Phys.* **32**(3), 510–519 (1961).
2. Friedman, D., "Progress and challenges for next-generation high-efficiency multijunction solar cells," *Current Opinion in Solid State and Materials Science* **14**(6), 131–138 (2010).
3. Guillemoles, J.-F., "Future concepts for photovoltaic energy conversion," in [*Fundamentals of Materials for Energy and Environmental Sustainability*], Ginley, D. S. and Cahen, D., eds., ch. 19, 238–256, Cambridge University Press (2011).
4. Luque, A. and Martí, A., "Increasing the efficiency of ideal solar cells by photon induced transitions at intermediate levels," *Phys. Rev. Lett.* **78**(26), 5014–5017 (1997).
5. Luque, A., Martí, A., and Stanley, C., "Understanding intermediate-band solar cells," *Nat Photon* **6**(3), 146–152 (2012).
6. López, N., Reichertz, L. A., Yu, K. M., Campman, K., and Walukiewicz, W., "Engineering the electronic band structure for multiband solar cells," *Phys. Rev. Lett.* **106**(2), 028701– (2011).
7. Ahsan, N., Miyashita, N., Islam, M. M., Yu, K. M., Walukiewicz, W., and Okada, Y., "Two-photon excitation in an intermediate band solar cell structure," *Appl. Phys. Lett.* **100**(17), 172111–4 (2012).
8. Wang, W., Lin, A. S., and Phillips, J. D., "Intermediate-band photovoltaic solar cell based on ZnTe:O," *Appl. Phys. Lett.* **95**(1), 011103 (2009).
9. Tanaka, T., Miyabara, M., Nagao, Y., Saito, K., Guo, Q., Nishio, M., Yu, K. M., and Walukiewicz, W., "Photocurrent induced by two-photon excitation in znteo intermediate band solar cells," *Appl. Phys. Lett.* **102**(5), 052111–4 (2013).
10. Winkler, M. T., Recht, D., Sher, M.-J., Said, A. J., Mazur, E., and Aziz, M. J., "Insulator-to-metal transition in sulfur-doped silicon," *Phys. Rev. Lett.* **106**(17), 178701– (2011).
11. Simmons, C. B., Akey, A. J., Krich, J. J., Sullivan, J. T., Recht, D., Aziz, M. J., and Buonassisi, T., "Deactivation of metastable single-crystal silicon hyperdoped with sulfur," *Journal of Applied Physics* **114**(24), 243514 (2013).
12. Bob, B. P., Kohno, A., Charnvanichborikarn, S., Warrender, J. M., Umezu, I., Tabbal, Malek Williams, J. S., and Aziz, M. J., "Fabrication and subband gap optical properties of silicon supersaturated with chalcogens by ion implantation and pulsed laser melting," *J. Appl. Phys.* **107**(12), 123506– (2010).
13. Persans, P. D., Berry, N. E., Recht, D., Hutchinson, D., Peterson, H., Clark, J., Charnvanichborikarn, S., Williams, J. S., DiFranzo, A., Aziz, M. J., and Warrender, J. M., "Photocurrent lifetime and transport in silicon supersaturated with sulfur," *Appl. Phys. Lett.* **101**(11), 111105–4 (2012).
14. Umezu, I., Warrender, J. M., Charnvanichborikarn, S., Kohno, A., Williams, J. S., Tabbal, M., Papazoglou, D. G., Zhang, X.-C., and Aziz, M. J., "Emergence of very broad infrared absorption band by hyperdoping of silicon with chalcogens," *J. Appl. Phys.* **113**(21), 213501–7 (2013).
15. Sánchez, K., Aguilera, I., Palacios, P., and Wahnón, P., "Assessment through first-principles calculations of an intermediate-band photovoltaic material based on ti-implanted silicon: Interstitial versus substitutional origin," *Phys. Rev. B* **79**(16), 165203–7 (2009).
16. Sánchez, K., Aguilera, I., Palacios, P., and Wahnón, P., "Formation of a reliable intermediate band in Si heavily coimplanted with chalcogens (S, Se, Te) and group III elements (B, Al)," *Phys. Rev. B* **82**(16), 165201– (2010).
17. Garcia-Hemme, E., Garcia-Hernansanz, R., Olea, J., Pastor, D., del Prado, A., Martil, I., and Gonzalez-Diaz, G., "Far infrared photoconductivity in a silicon based material: Vanadium supersaturated silicon," *Appl. Phys. Lett.* **103**(3), 032101–5 (2013).
18. Garcia-Hemme, E., Garcia-Hernansanz, R., Olea, J., Pastor, D., del Prado, A., Martil, I., and Gonzalez-Diaz, G., "Sub-bandgap spectral photo-response analysis of Ti supersaturated Si," *Appl. Phys. Lett.* **101**(19), 192101–5 (2012).

19. Olea, J., del Prado, A., Pastor, D., Mártil, I., and González-Díaz, G., "Sub-bandgap absorption in Ti implanted Si over the Mott limit," *J. Appl. Phys.* **109**(11), 113541 (2011).
20. Wahnón, P., Conesa, J. C., Palacios, P., Lucena, R., Aguilera, I., Seminovski, Y., and Fresno, F., "V-doped SnS₂: a new intermediate band material for a better use of the solar spectrum," *Phys. Chem. Chem. Phys.* **13**(45), 20401–20407 (2011).
21. Wahnón, P. and Tablero, C., "Ab initio electronic structure calculations for metallic intermediate band formation in photovoltaic materials," *Phys. Rev. B* **65**(16), 165115– (2002).
22. Lucena, R., Aguilera, I., Palacios, P., Wahnón, P., and Conesa, J. C., "Synthesis and spectral properties of nanocrystalline V-substituted In₂S₃, a novel material for more efficient use of solar radiation," *Chemistry of Materials* **20**(16), 5125–5127 (2008).
23. Aguilera, I., Palacios, P., and Wahnón, P., "Enhancement of optical absorption in Ga-chalcopyrite-based intermediate-band materials for high efficiency solar cells," *Solar Energy Materials and Solar Cells* **94**(11), 1903–1906 (2010).
24. Palacios, P., Aguilera, I., Sánchez, K., Conesa, J. C., and Wahnón, P., "Transition-metal-substituted indium thiospinels as novel intermediate-band materials: Prediction and understanding of their electronic properties," *Phys. Rev. Lett.* **101**(4), 046403–4 (2008).
25. Strandberg, R. and Aguilera, I., "Evaluation of vanadium substituted In₂S₃ as a material for intermediate band solar cells," *Solar Energy Materials and Solar Cells* **98**(0), 88–93 (2012).
26. Krich, J. J., Halperin, B. I., and Aspuru-Guzik, A., "Nonradiative lifetimes in intermediate band photovoltaics—absence of lifetime recovery," *J. Appl. Phys.* **112**(1), 013707–8 (2012).
27. Sullivan, J. T., Simmons, C. B., Krich, J. J., Akey, A. J., Recht, D., Aziz, M. J., and Buonassisi, T., "Methodology for vetting heavily doped semiconductors for intermediate band photovoltaics: A case study in sulfur-hyperdoped silicon," *Journal of Applied Physics* **114**(10), 103701 (2013).
28. Ley, M., Boudaden, J., and Kuznicki, Z. T., "Thermodynamic efficiency of an intermediate band photovoltaic cell with low threshold auger generation," *J. Appl. Phys.* **98**(4), 044905–5 (2005).
29. Luque, A., Marti, A., Lopez, N., Antolin, E., Canovas, E., Stanley, C., Farmer, C., and Diaz, P., "Operation of the intermediate band solar cell under nonideal space charge region conditions and half filling of the intermediate band," *J. Appl. Phys.* **99**(9), 094503–9 (2006).
30. Navruz, T. and Saritas, M., "Efficiency variation of the intermediate band solar cell due to the overlap between absorption coefficients," *Solar Energy Materials and Solar Cells* **92**(3), 273–282 (2008).
31. Lin, A. S., Wang, W., and Phillips, J. D., "Model for intermediate band solar cells incorporating carrier transport and recombination," *Journal of Applied Physics* **105**(6), 064512 (2009).
32. Lin, A. and Phillips, J., "Drift-diffusion modeling for impurity photovoltaic devices," *Electron Devices, IEEE Transactions on* **56**(12), 3168–3174 (2009).
33. Strandberg, R. and Reenaas, T. W., "Drift-diffusion model for intermediate band solar cells including photofilling effects," *Prog. Photovolt: Res. Appl.* **19**(1), 21–32 (2011).
34. Nelson, J., [*The Physics of Solar Cells*], Imperial College Press (2003).
35. Gray, J. L., "The physics of the solar cell," in [*Handbook of Photovoltaic Science and Engineering, Second Edition*], Luque, A. and Hegedus, S., eds., ch. 3, 82–129, Wiley (2011).
36. Synopsys Inc., Mountain View, CA, USA, *Sentaurus Device User Guide, Version G-2012.06* (2012).
37. Walker, A. W., Thériault, O., and Hinzer, K., "The dependence of multi-junction solar cell performance on the number of quantum dot layers," *IEEE Journal of Quantum Electronics* (forthcoming).
38. Walker, A. W., Thériault, O., and Hinzer, K., "Positioning and doping effects on quantum dot enhanced multi-junction solar cell performance," *Progress in Photovoltaics* (forthcoming).
39. Sotoodeh, M., Khalid, A. H., and Rezazadeh, A. A., "Empirical low-field mobility model for III-V compounds applicable in device simulation codes," *Journal of Applied Physics* **87**(6), 2890–2900 (2000).